Modelling the impact of HIF on metabolism and the extracellular matrix: consequences for tumour growth and invasion

Kévin Spinicci, Gibin Powathil, Angélique Stéphanou

Modelling the impact of HIF on metabolism and the extracellular matrix: consequences for tumour growth and invasion.

Kévin Spinicci[1,2], Gibin Powathil[2], and Angélique Stéphanou[1]

[1]Univ. Grenoble Alpes, CNRS, UMR 5525, VetAgro Sup, Grenoble INP, TIMC, 38000 Grenoble, France

[2]Department of Mathematics, Swansea University, Swansea, SA1 8EN, United Kingdom

October 3, 2024

Abstract

The extracellular matrix (ECM) is a complex structure involved in many biological processes with collagen being the most abundant protein. Density of collagen fibers in the matrix is a factor influencing cell motility and migration speed. In cancer, this affects the ability of cells to migrate and invade distant tissues which is relevant for designing new therapies. Furthermore, increased cancer cell migration and invasion have been observed in hypoxic conditions. Interestingly, it has been revealed that the Hypoxia Inducible Factor (HIF) can not only impact the levels of metabolic genes but several collagen remodeling genes as well. The goal of this paper is to explore the impact of the HIF protein on both the tumour metabolism and the cancer cell migration with a focus on the Warburg effect and collagen remodelling processes. Therefore, we present an agent-based model (ABM) of tumour growth combining genetic regulations with metabolic and collagen-related processes involved in HIF pathways. Cancer cell migration is influenced by the extra-cellular collagen through a biphasic response dependant on collagen density. Results of the model showed that extra-cellular collagen within the tumour was mainly influenced by the local cellular density while collagen also influenced the shape of the tumour. In our simulations, proliferation was reduced with higher extra-cellular collagen levels or with lower oxygen levels but reached a maximum in the absence of cell-cell adhesion. Interestingly, combining lower levels of oxygen with higher levels of collagen further reduced the proliferation of the tumour. Since HIF impacts the metabolism and may affect the appearance of the Warburg Effect, we investigated whether different collagen conditions could lead to the adoption of the Warburg phenotype. We found that this was not the case, results suggested that adoption of the Warburg phenotype seemed mainly controlled by inhibition of oxidative metabolism by HIF combined with oscillations of oxygen.

Introduction

The extracellular matrix (ECM) is a complex structure that can dictate the behaviour of the cell by influencing its proliferation, growth, migration and apoptosis. While its composition can greatly vary between tissues, it contains 300 types of proteins, water, polysaccharides and proteoglycans. ECM proteins can influence tissue homeostasis, organ development, inflammation and diseases. Most of these proteins are fibrous proteins like collagen, elastin, fibronectin and laminin [1]. Cell migration direction and speed can be influenced by the ECM stiffness, *i. e.* its resistance to deformation in response to applied forces. Motility and invasion, ability to proliferate and colonize other tissues are among the essential hallmarks of metastatic cells [2].

These hallmarks are influenced by collagen: the most abundant fibrous protein. Fibroblasts represent the main source of collagen and are responsible for both the organization and the alignment of collagen fibres. Mutations of collagen have been associated with diseases like osteoporosis. The collagen family includes 28 different collagen types classified into seven different categories [3]. The synthesis of collagen is a complex process that involves several post-translational modifications and the assembly of pro-collagen chain, secretion and processing to form the collagen fibres network [4]. Literature has demonstrated that three families of genes that are involved in the collagen modification of the ECM: the prolyl 4-hydroxylase (P4H), matrix metalloproteinases (MMPs) and the lysyl oxidase (LOX) [5, 6, 7, 8]. Cell-fibres interactions represent a major component for cell migration as cells are slower in stiffer matrix, yet they tend to migrate to stiff areas of the matrix [9]. In cancer, enhanced deposition of collagen is the most recognized alteration of tumorous tissues. Cancer cells are able to stimulate the synthesis of ECM proteins through cancer associated fibroblast (CAF) recruitment. Increased deposition of collagen has been observed in hypoxic areas of the tumour [5].

Hypoxia is a major phenomenon observed in cancer as the median observed tumour oxygen is 2 % [10]. In glioblastoma, the inconsistent oxygenation due to the altered blood vessels causes hypoxia, increased acidity and necrosis [11]. The increased resistance to radiotherapy of hypoxic cells was attributed to the Hypoxia Inducible Factor (HIF) [12]. The HIF protein is the main actor involved in the cellular response to hypoxia. The most known isoform HIF1-α acts as a transcription factor that can up-regulate the transcriptional activity of target genes called hypoxia response elements (HRE). 98 genes have been identified as HRE [13]. They are involved in various biological functions such as cell proliferation, survival, apoptosis, erythropoiesis and angiogenesis [14]. HIF is mainly regulated at the protein level by oxygen-dependant degradation mechanisms [15]. It can affect the levels of the two metabolic genes lactate dehydrogenase (LDH) and pyruvate dehydrogenase (PDH) [16, 14]. Hence, HIF may be a regulator of the Warburg Effect which is characterized by an increased production of lactate (even in normoxia) induced by an increased usage of the glycolytic pathways. HIF1-α has been recognized as a master regulator of the epithelial to mesenchymal transition (EMT), invasion and metastasis in breast cancer [17]. Exposure of cells to hypoxia in glioblastoma elevated the levels of EMT associated genes [18]. Interestingly, high matrix stiffness can inhibit angiogenesis [7].

Because metastasis is a major factor hindering therapy in cancer, cell migration has been studied

through mathematical modeling which included different processes such as collagen degradation, cell-cell adhesion or the effect of a heterogeneous matrix [19, 20, 1, 21, 22]. It should be noted that the processes mentioned are occuring at the early stage of the metastatic process while, in later stages, the cell escapes its original tissue and starts invading surrounding ones. Among the models of cellular migration mentioned above, none investigated the effect of HIF on migration despite hypoxia being a common factor in cancer which promotes invasion. While HIF has been mathematically described, it was mainly to understand its biology (*e. g.* its regulation by oxygen-dependant mechanisms) using ordinary differential equations (ODEs) based systems (see [23, 24, 25, 26]).

In a previous study, we investigated the effect of HIF on the Warburg Effect through its impact on the LDH and PDH genes in the case of glioblastoma. We have shown that the Warburg phenotype could be triggered when the oxygen-dependant degradation of HIF was reduced or when oxygen diffusion varied through the tumour growth [27].

While the ECM in the brain lacks rigid structure such as fibrous protein [28], it has been observed that the matrix in glioblastoma has a higher collagen content than in a healthy brain [1]. In progressive glioma, the brain matrix becomes more disorganized and stiffer with the growing malignancy of the tumour [2]. Furthermore, it has been shown that glioblastoma cells are able to produce collagen fibres like fibroblasts [29, 30]. Hence in this paper, we present a mathematical model of the impact of HIF on cellular migration through its effect on collagen remodeling processes in the case of glioblastoma. We developed an agent-based model (ABM) to characterize the interaction between the cell and the ECM at the cellular level. Modification of the collagen content is influenced by the level of HIF. The model describes the impact of collagen on the cell migration speed, to reflect the differences between tumour growth in different collagen conditions.

Materials and Methods

Existing model

The model presented in this paper is based on our precedent work on the study of the impact of HIF on the metabolic key genes LDH and PDH [27]. The levels of LDH and PDH enzymes control the usage of aerobic and anaerobic pathways to produce the cell's Adenosine Triphosphate (ATP). The paper aimed to study how different levels of HIF can lead to the appearance of the Warburg effect during tumour growth in different conditions. The model combined a gene regulatory network with equations for metabolism influenced by the levels of LDH and PDH described by ODEs:

$$\frac{dh}{dt} = \alpha_h \ \beta_h - d_h \ S(O, s_{O\to h}, \gamma_{O\to h}) \ h, \tag{1}$$

$$\frac{dl}{dt} = \alpha_l \ S(h, s_{h\to l}, \gamma_{h\to l}) - d_l \ l, \tag{2}$$

$$\frac{dk}{dt} = \alpha_k \ S(h, s_{h\to k}, \gamma_{h\to k}) - d_k \ k, \tag{3}$$

$$\frac{dq}{dt} = \alpha_q \ S(k, s_{k\to q}, \gamma_{k\to q}) - d_q \ q, \tag{4}$$

with h, l, k and q the levels of HIF, LDH, PDK and PDH. Gene regulations were simulated using the Shifted-Hill function [31], a non-linear function to depict gene up- and down- regulation depending on a regulating gene. The Shifted-Hill function consists mainly of the summation of two Hill terms:

$$S(Y, s, \gamma) = \frac{s^n}{s^n + Y^n} + \gamma \frac{Y^n}{s^n + Y^n}. \tag{5}$$

Here n is the Hill coefficient, s is the level of the regulating protein Y at which the regulation is half-maximum, γ is the regulating strength of Y on its target with $\gamma \in \mathbb{R}_+$. If $\gamma > 1$ then $S(Y, s, \gamma)$ indicates an up-regulation, if $\gamma < 1$ then $S(Y, s, \gamma)$ indicates a down-regulation.

Metabolism is mainly simulated using Michaelis-Menten function [32]. The model described extracellular quantities of oxygen, glucose and H^+ through partial differential equations (PDEs):

$$\frac{\partial O}{\partial t} = D_O \nabla^2 O - \sum_{N}^{i=1} f_O^i, \tag{6}$$

$$\frac{\partial G}{\partial t} = D_G \nabla^2 G - \sum_{N}^{i=1} f_G^i, \tag{7}$$

$$\frac{\partial H}{\partial t} = D_H \nabla^2 H + \sum_{N}^{i=1} f_H^i. \tag{8}$$

With D_O, D_G and D_H the diffusion coefficients of the different diffusibles. f_O and f_G are functions describing the consumption of oxygen and glucose, respectively, while f_H determines the secretion of protons. Here, we sum the consumption and secretion f^i for each cell i to N in the current voxel.

Generation of ATP at each timestep:

$$\frac{dA}{dt} = f_A. \tag{9}$$

See (14) for more details on ATP generation.

Oxygen (O) consumption:

$$f_O = \Psi_O V_O \frac{O}{K_O + O}, \tag{10}$$

$$\Psi_O = \frac{\Phi_O - \phi_O}{1 + \exp\left(-\lambda_q (q - q_0) \right)} + \phi_O. \tag{11}$$

V_O is the maximal consumption rate of oxygen and K_O is the concentration of oxygen at which the consumption is half-maximal (Michaelis-Menten constant of oxygen). Ψ_O is a logistic function to tune the consumption of oxygen depending on the level of the gene PDH. Φ_O and ϕ_O represent the maximum and minimum values, λ_q is the steepness of the curve, q is the level of PDH and q_0 is the level at which the effect of PDH is half-maximal (midpoint of the logistic curve, similar to the Michaelis-Menten constant).

Glucose (G) consumption:

$$f_G = \left(\frac{\Psi_G A_0}{2} - \frac{29 f_O}{10} \right) \frac{G}{K_G + G}, \tag{12}$$

$$\Psi_G = \frac{\Phi_G - \phi_G}{1 + \exp\left(-\lambda_l (l - l_0) \right)} + \phi_G. \tag{13}$$

A_0 is the target ATP demand the cell needs to meet, K_G is the concentration of glucose at which the consumption is half-maximal. Glucose consumption is influenced through the term Ψ_G which represents the effect of the LDH gene on glucose consumption. Φ_G and ϕ_G represent the maximum and minimum

values, λ_l is the steepness of the curve, l is the level of LDH and l_0 is the level at which the effect of LDH is half-maximal.

ATP (A) production:

$$f_A = 2f_G + \frac{29}{5} f_O. \tag{14}$$

Here, levels of ATP generated are computed from the consumption of glucose and oxygens multiplied by their respective stoichiometric coefficients.

H^+ (H) secretion:

$$f_H = 2f_G \; k_H. \tag{15}$$

k_H is a proton-buffering term.

Accurate depiction of oxygen diffusion would lead to a better representation of HIF levels within the tumour. Thus we developed an ABM using the PhysiCell software [33], a C++ software designed to run simulations of tumour growth for a large population of cells. The software displays good performance with low memory footprint and fast simulation thanks to parallelized computation. Cell state in the model was updated at each $dt_{phenotype}$ using the level of ATP generated at each timestep and the local extracellular pH. If levels of ATP or pH generated were too low, the cell dies. If pH was sufficient and the levels of ATP generated were high enough for the cell to survive but not enough for division, then the cell enters quiescience. Lastly, if levels of ATP generated were high and pH was not too low, then the cell is allowed to divide with no conditions on the cell neighborhood.

Effect of HIF on the nature and content of collagen

Collagen is a molecule that undergo complex post-translational modification which modifies its properties as well as the properties of the resulting ECM [5]. While ECM in the brain is known to lack rigid structures [28], brain in glioblastoma has a higher collagen content [2] with a stiffer and more disorganized matrix than healthy brain [34]. Hence, in this paper, we focus on the action of three different families of proteins namely of the P4Hs family, MMPs family and LOXs family impacting the formation, degradation and cross-linking of collagen fibres [7, 6, 8]. These families were selected due to their up-regulation by HIF.

Proline residues of procollagen are hydroxylated by members of the P4H which is an essential step for the proper folding of collagen chains enabling them to form a triple helical structure, promoting the formation of collagen fibres. P4HA1 and P4HA2, two P4H isoforms, are found to be up-regulated by HIF1-α [11, 35, 34, 36, 37]. Yet we only modelled the P4HA1 isoform as no differences between the two proteins were documented.

Cancer cell migration is favoured by matrix degradation creating available space for the cell to migrate into. Many molecules can degrade collagen such as the "A disintegrin and metalloproteinases (ADAM)" family and cathepsins [38, 39, 40, 41]. Yet, the main collagen degradation activity is attributed to a family of Zn^{2+} dependent edopeptidases called matrix metalloproteinases (MMPs). Various MMP isoforms have been identified, among them MMP2/MMP9 and MT1-MMP (also called MMP14) have been observed to be up-regulated by HIF [5, 36, 42, 43, 44, 45, 46]. Despite that MMP2 and MMP9 are considered to be oncogenes [47, 48, 40], only MT1-MMP is included in the model, a choice motivated by several

reasons. The activity of several MMPs is redundant and compensatory, hence modelling several MMPs would not give more accurate results and would increase the complexity of the model. In addition, MMP2 activation is dependent on the tissue inhibitors of MMP (TIMP)-2 factor and MT1-MMP [49, 50, 51], suggesting that MT1-MMP would be a limiting factor for MMP2 activation. Furthermore, MT1-MMP could promote cellular invasiveness but not soluble MMPs [49]. Lastly, MMP2 collagenolytic activity seems to be ambiguous. MMP2 may be important for the clearance of degraded and denatured collagen partially cleaved by MT1-MMP beforehand [39, 41].

Cross-linking of collagen fibrils by LOX stabilizes the collagen fibrils which gives collagen its tensile strength and mechanical stability [4]. HIF is able to up-regulate three members of the LOX family, here we include only the activity of the LOX gene as it seems that cross-linking activity is most often attributed to this isoform.

The effects of the different genes on collagen described here are summarized in figure 1.

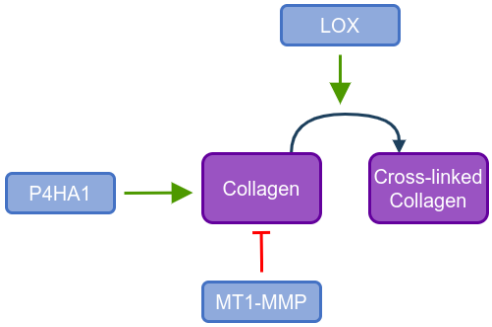

Figure 1: Secretion, degradation and cross-linking of collagen mediated by P4H1A, MT1-MMP and LOX.

Gene levels are described using the following set of ODE:

$$\frac{dp}{dt} = \alpha_p \; S(h, s_{h\to p}, \gamma_{h\to p}) - d_p \; p, \tag{16}$$

$$\frac{dm}{dt} = \alpha_m \; S(h, s_{h\to m}, \gamma_{h\to m}) - d_m \; m, \tag{17}$$

$$\frac{dr}{dt} = \alpha_r \; S(h, s_{h\to r}, \gamma_{h\to r}) - d_r \; r, \tag{18}$$

where p, m and r describe the levels of P4HA1, MT1-MMP and LOX. Here, α_x is the production rate of the protein x and d_x is the degradation rate of the protein x. Up-regulation of P4HA1, MT1-MMP and LOX by HIF are described using the Shifted-Hill equation (Equation 5).

Parameters for the Shifted-Hill equation were estimated using glioblastoma bulk tumour RNA-Seq data from the TCGA-GBM project available on the The Cancer Genome Atlas (TCGA) database. Parameters were normalized as follows:

1. Normalization of the count data using the `normTransform` function from the DESeq2 R package [52] (version 1.40).

2. Interpolation of normalized values:

$$\hat{x} : f(x) = \frac{x - x_{min}}{x_{max} - x_{min}}, \text{ with } \hat{x} \in [0, 1].$$

3. The Shifted-Hill function is the summation of two Hill terms: an activating term and an inhibiting one. Only the activating term is effective when $\gamma > 1$ (when Y up-regulates X), while only the inhibiting term is effective when $\gamma < 1$ (when Y down-regulates X). Therefore, we use this property to fit the parameter s on different functions depending on the value of γ:

$$h(Y) = \frac{Y^n}{s^n + Y^n}, \text{ if } \gamma > 1 \text{(up-regulation)}$$
$$h(Y) = \frac{s^n}{s^n + Y^n}, \text{ if } \gamma < 1 \text{(down-regulation)}$$

Y is the regulating gene, n is the Hill coefficient, s is the concentration of Y at which the effect on X is half-maximal. The Hill coefficient is fixed to 4, the value used in the model.

4. The parameter s is then rescaled to the original dimensions of the data before Interpolation.

5. The γ parameter is estimated using the fold-change of expression in the data:

$$\text{fold-change} = \frac{x_{max}}{x_{min}}, \text{if the gene } X \text{ is up-regulated,}$$
$$\text{fold-change} = \frac{x_{min}}{x_{max}}, \text{if the gene } X \text{ is down-regulated.}$$

Initial protein level were set to 1.0 in every simulations ran. Parameters for genetic regulation are summarised in table 1.

Parameter	Value	Dimension	Parameter	Value	Dimension
$\alpha_h, \alpha_l, \alpha_k, \alpha_q, \alpha_p, \alpha_m, \alpha_r$	0.005	min^{-1}	$d_h, d_l, d_k, d_q, d_p, d_m, d_r$	0.005	min^{-1}
$s_{O\to h}$	0.02085	mmol/L	$s_{h\to l}$	13.04	-
$s_{h\to k}$	13.34	-	$s_{k\to q}$	9.94	-
$s_{h\to p}$	13.68	-	$s_{k\to m}$	13.25	-
$s_{h\to r}$	13.44	-			
$\gamma_{O\to h}$	25.01	-	$\gamma_{h\to l}$	16.06	-
$\gamma_{h\to k}$	17.87	-	$\gamma_{k\to q}$	0.78	-
$\gamma_{h\to p}$	16.87	-	$\gamma_{k\to m}$	20.43	-
$\gamma_{h\to r}$	25.46	-			
β_h	25.01	-	n	4	-

Table 1: Parameters for genetic regulations in the model of the impact of HIF on the cellular invasion. The symbol "-" stands for dimensionless.

Implementation of the ECM and collagen modifying processes

The PhysiCell software simulates the microenvironment of the cell as a 2D square-grid lattice. Each element of the grid is called a voxel, extracellular quantities vary between each voxel. The ECM is not explicitly modeled in PhysiCell, instead we describe the extra-cellular collagen as a substrate that does

not diffuse nor decay. Extensive characterization of collagen through complete mechanical interaction or modeling of the fibres is out of the scope of this study. This study aims to characterize instead the variations of collagen content caused by HIF. Modelling collagen as a substrate still retains the ability to describe different states of collagen namely "collagen" and "cross-linked collagen". Cross-linked collagen participates in the matrix stiffness yet it is resistant to degradation by MMP [39, 41].

Collagen fibres are composed of several procollagen α chains coded by the COL genes (COL1A1, COL1A3, etc). These chains undergo post-translational modification by P4Hs proteins which favour the assembling of procollagen into collagen fibres. We hypothesize that the formation of collagen fibres is dependent upon the activity of P4HA1, since unprocessed procollagen does not form any collagen fibres and consequently, does not participate in the collagen content of the ECM. As for secretion, collagen degradation and cross-linking are influenced by the levels of MT1-MMP and LOX. Compared to the secretion of collagen, processes of degradation and cross-linking require collagen fibres as a substrate. Consequently, degradation/cross-linking should not only rise as enzyme levels increase but fall as collagen quantity decreases as well. Collagen degradation and cross-linking are modeled using Michaelis-Menten dynamics. MT1-MMP activity has already been described using Michaelis-Menten dynamics in the literature [50]. The resulting functions to describe collagen dynamics are:

$$f_C = \beta_p p - \beta_m m \frac{C}{K_m + C} - \beta_r r \frac{C}{K_r + C}, \tag{19}$$

$$f_{C_r} = \beta_r r \frac{C}{K_r + C}, \tag{20}$$

where f_C and f_{C_r} describe the variations of collagen C and cross-linked collagen C_r in the environment. Levels of P4HA1, MT1-MMP and LOX are described by the variables p, m and r. Parameters β_p, β_m and β_r are the base rate of collagen secretion, degradation by m and cross-linking by r. K_m is the level of m at which the degradation rate of collagen is half-maximal, and K_r is the level of r at which the cross-linking rate is half-maximal.

While degradation of the ECM is essential for cellular migration, ECM acts as an important scaffolding for migration, hence its degradation must be localized [49]. MT1-MMP is a membrane-bound protein usually located on the invadopodia or lamellipodia: the migration front of the cell [50, 49]. Consequently, the distance of MT1-MMP mediated degradation should be limited by the cell in the model. The cell will only degrade the collagen of the voxel it is currently inside. For simplicity of implementation, LOX-mediated cross-linking will follow the same rule. PhysiCell does not have built-in interaction between substances; which means that it does not describe any interactions of the type "the **Substance A** influences the concentration of a **Susbtance B**". Hence, interactions between extracellular LOX and collagen would need to be implemented manually. The unit to quantify the density of collagen and cross-linked collagen is mg/mL, the unit the most often reported when conducting gel experiments. The extracellular density of collagen is described by the PDEs:

$$\frac{\partial C}{\partial t} = \sum_{N}^{i=1} f_C^i, \tag{21}$$

$$\frac{\partial C_r}{\partial t} = \sum_{N}^{i=1} f_{C_r}^i. \tag{22}$$

Here f_C^i and $f_{C_r}^i$ are the quantity of collagen degraded and the quantity of collagen cross-linked by the cell i, N is the total number of cell in the current voxel.

Let x_0 and y_0 the lower boundary of the domain in x and y, x_L and y_L the upper boundary in x and y. Simulations were run with the following initial conditions:

- Oxygen: $O(x, y, 0) = 0.056$ mmol/L (normoxia or 5 % O_2) [10].
- Glucose: $G(x, y, 0) = 5.0$ mmol/L (serum glucose) [53].
- H^+ : $H^+(x, y, 0) = 3.98 \times 10^{-5}$ mmol/L (pH 7.4).
- Collagen: $C(x, y, 0) = 2.5$ mg/mL (optimal collagen density for growth [54]).
- Cross-linked Collagen: $C_r(x, y, 0) = 0.0$ mg/mL.

And the following Dirichlet-Boundary conditions:

- Oxygen: $O(x_0, y, t) = O(x_L, y, t) = O(x, y_0, t) = O(x, y_L, t) = 0.056$ mmol/L.
- Glucose: $G(x_0, y, t) = G(x_L, y, t) = G(x, y_0, t) = G(x, y_L, t) = 5.0$ mmol/L.
- H^+ : $H^+(x_0, y, t) = H^+(x_L, y, t) = H^+(x, y_0, t) = H^+(x, y_L, t) = 3.98 \times 10^{-5}$ mmol/L (pH 7.4).
- Collagen and Cross-linked collagen: No boundary conditions as they do not diffuse.

The list of parameters for the model can be found in table 2.

Integration of cell migration

ECM collagen content is an important factor that influences both the ability of the cell to migrate and its speed [55]. Experiments of cellular migration on collagen gels with different properties show a biphasic effect of collagen on the migration speed of the cell [54, 56]. Studies report that the cellular migration speed in different collagen densities is a bell-shaped curve. At the beginning, the speed of the cell increases with higher collagen densities until a maximum is reached, which is reported to be 1.2 or 2.0 mg/mL of collagen [54, 56]. After that maxima, the cell migration speed decreases as collagen densities continue to rise. In addition, it has been observed that cells are less invasive in a softer matrix (0.5 mg/mL of collagen) [29]. Following the observation made by Schor et *al* [54], we only allow cellular migration for collagen densities between 0.5 and 4.0 mg/mL. We fitted a second-degree polynomial using their data with values in $[0, 1]$ to modify the speed of the cell from 0 up to a maximum. Data were normalized between 0 and 1 prior to fitting. Figure 2 shows the result of the fit and the impact of collagen.

The speed of the cell is represented by the following piecewise function :

$$\nu = \begin{cases} 0 & \text{if } C_t \notin [0.5, 4.0] \text{ mg/mL}, \\ \nu_0(-0.23x^2 + 0.971x - 0.048) & \text{if } C_t \in [0.5, 4.0] \text{ mg/mL}, \end{cases} \tag{23}$$

where ν_0 is the base speed of the cell and C_t the total density of collagen ($C_t = C + C_r$). Here ν_0 is equal to 0.8 µ m/min [29].

Parameter	Value	Unit	Description
Oxygen			
V_O	0.01875	$mmol/L/min$	Maximal oxygen consumption rate
K_O	0.0075	$mmol/L$	Michaelis-Menten constant of oxygen consumption
Φ_O	1	-	Maximum value of Ψ_O
ϕ_O	0	-	Minimum value of Ψ_O
λ_q	15	-	Steepness of Ψ_O
q_0	0.575	-	Midpoint of Ψ_O
Glucose			
K_G	0.04	$mmol/L$	Michaelis-Menten constant of glucose consumption
A_0	0.10875	$mmol/L/min$	Target ATP level
Φ_G	50	-	Maximum value of Ψ_G
ϕ_G	1	-	Minimum value of Ψ_G
λ_l	4	-	Steepness of Ψ_G
l_0	8.03	-	Midpoint of Ψ_G
H^+			
K_H	$2.5 \cdot 10^{-4}$	-	Proton buffering term
collagen			
β_p	4.04×10^{-6}	$mg/mL/min$	Base collagen secretion rate by P4HA1
β_m	2.16×10^{-5}	$mg/mL/min$	Base collagen degradation rate by MT1-MMP
K_m	8.7×10^{-11}	mg/mL	Michaelis-Menten constant of MT1-MMP
β_r	2.91×10^{-10}	$mg/mL/min$	Base collagen cross-linking rate by LOX
K_r	6.75×10^{-9}	mg/mL	Michaelis-Menten constant of LOX
Diffusion			
D_O	$109,200$	$\mu m^2/min$	Oxygen diffusion coefficient
D_G	$30,000$	$\mu m^2/min$	Glucose diffusion coefficient
D_{H^+}	$27,0000$	$\mu m^2/min$	H^+ diffusion coefficient

Table 2: Parameters for metabolism. The symbol "-" stands for dimensionless.

Results

Extra-cellular collagen within the tumour is impacted by the local cellular density

A simulation was run with default parameters and initial conditions: homogeneous and normoxic oxygen conditions with a homogeneous collagen matrix at a concentration optimal for growth. Figure 3 shows the resulting tumour along with the extracellular collagen and the cellular density within the tumour. After 14 days of growth, the center of the tumour is mainly composed of necrotic cells while the periphery is composed of proliferative cells. A thin layer of quiescent cells can be observed between the necrotic cells and the proliferative cells. This layer is thicker at the bottom of the tumour compared to the top.

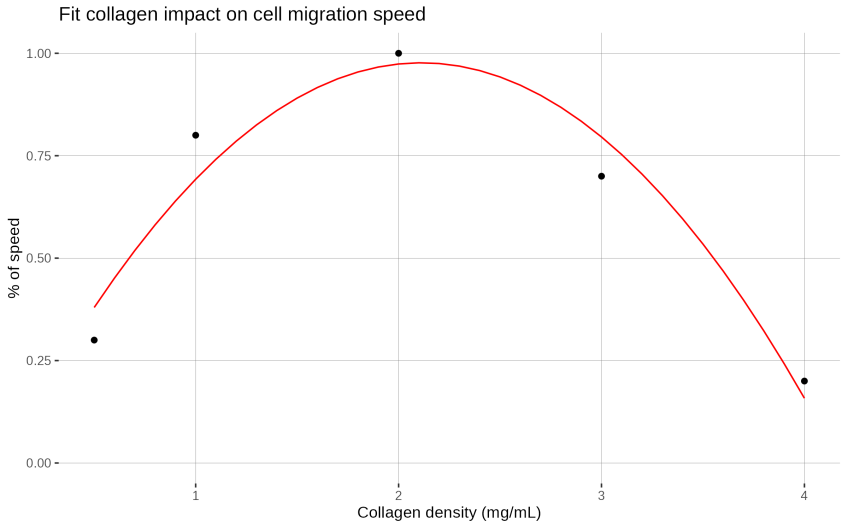

Figure 2: Result of the fit of a second-degree polynomial on the data from Schor et *al* [54].

On the opposite, a group of necrotic swelling cells is present on the upper part of the tumour.

Some cells tend to detach from the tumour's main body and move slightly away, although it is not significant enough to call those cells "invasive". This observation is similar to the results from Rubenstein et *al* [22] with their model of cell migration based on a cellular Potts model. Because collagen is an important aspect of the model, it appears essential to investigate how the tumour impacts extracellular collagen density. Collagen density within the tumour ranges from 0 to 2.0 mg/mL. The highest density of collagen inside the tumour is found at its centre where tumour growth started. At the beginning of the simulation, cells are in normoxia and may not alter much the collagen content. Because cells at the centre of the tumour are the first to die due to harsh conditions, they may not had the time to alter significantly their environment.

Interestingly, the pattern of extracellular collagen is similar to the pattern of the local cellular density and the cellular migration speed. Areas with higher local cellular density display decreased extracellular collagen levels and cellular migration speed. This suggests that a higher number of cells leads to an increased degradation of collagen which affects the cellular migration speed. Consequently, cellular migration speed decreases when the cellular density rises. The reason why cellular density locally rises is unknown. However, it could be explained by the asynchronicity of the cell cycle. The cell cycle phase is randomized at the beginning of the simulation to replicate more accurately the growth that could be observed *in vivo*. Thus, a few cells may divide more early than others cells as they are in a later stage of the cell cycle which increases the local cellular density.

Tumour proliferation is impacted by extracellular collagen, oxygen and cellular adhesion forces

To understand the impact of environmental collagen and oxygen on tumour growth, different environmental settings were tested:

- Bi-Gel: The microenvironment is split into two collagen densities like a collagen gel with a soft

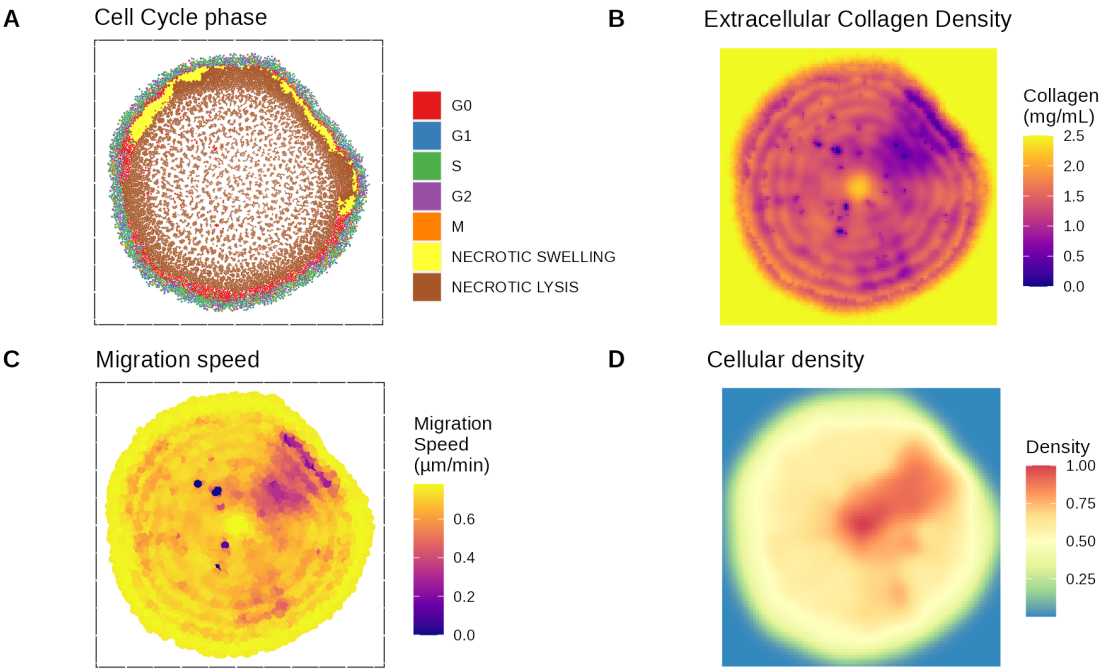

Figure 3: Tumour after 14 days grew in normoxia with the default initial conditions and parameters. The figure shows the (A) cell-cycle phase, (B) extracellular collagen, (C) migration speed and (D) normalized cellular density within the tumour.

part (2.5 mg/mL) and a stiff one (5.0 mg/mL) to assess the impact two densities may have on the tumour.

- Lower/Upper Oxygen: Oxygen only diffuses at the top and the bottom of the domain to determine how cells with lower access to oxygen respond.
- Bi-Gel + Lower/Upper Oxygen: Combination of the Bi-Gel condition and the Lower/Upper Oxygen settings to observe the impact of both conditions.
- Complex matrix: Collagen density is randomly generated following a uniform distribution between 0.5 and 4.0 mg/mL to simulate a heterogeneous environment comparable to *in vivo* conditions.
- No Cell-Cell adhesion: In that case, cell-cell adhesion forces are null as migrating cells are known to have reduced cell-cell adhesion and increased cell-matrix interactions. Cellular adhesion forces can be controlled through a parameter defined in the PhysiCell software.

Figure 4 graphically describes the different collagen and oxygen settings used. Tumour growth after 14 days in these different conditions is shown in figure 5. Like in the reference, the tumour in every simulation is composed of a necrotic core with a surrounding layer of proliferative cells. Interestingly, cells tend to pack together when dying in the necrotic core of the majority of simulations run except in the simulation with no cell-cell adhesion. With no cellular adhesion, the cell spatial distribution shows the same wave pattern as extracellular collagen in figure 3, similar to the results generated by the model from Anderson [20]. The tumour has a “roundish” shape in the reference, it has a “pear” shape in the

Bi-Gel and seems to form some branching in the complex matrix. Formation of "branching-like" structure is also observed in the model from Anderson [20] yet in the latter, these structures are more pronounced than in our results. In Anderson's model, the tumour is grown for a longer time than in this study which may explain why the results are different. The results obtained in different collagen conditions suggest that extracellular collagen only is able to shape the tumour during growth. This may be explained by the differences in migration speed among the cells caused by different collagen conditions.

Figure 6 shows the extracellular collagen, extracellular oxygen, cellular density and the cell migration speed in the different simulations after 14 days of growth. Similar to the observations with the reference simulation (figure 3), the matching pattern indicates a possible link. As can be observed, regions with lower migration speed values colocate with hollow areas where the "branches" of the tumour are forming. As a result, areas with lower collagen levels result in decreased cell migration speed which affect the shape of the tumour.

Collagen density within the tumour displays a pattern composed of circles, like a travelling wave. This may be caused by successive cell division: when cells divide, they push each other away, distributing them in circles as the tumour grows rather than uniformly. From the figure 6, it is possible to see areas with lower extracellular collagen within the tumour. This pattern does appear clearly in the reference simulation (figure 6.A.i) and in the case with no cell adhesion (figure 6.A.vi). In the case with bi-gel (figure 6.A.ii), this pattern seems more pronounced in the lower part of the tumour where collagen density is closer to optimal values than in the upper part corrsponding to stiffer matrix. Similarly, the pattern does not seems visible in the case with no oxygen diffusing from the left and right borders of the domain (figure 6.A.iii). This pattern seems present in the simulation with an heterogeneous matrix (figure 6.A.v) but it is harder to visually differentiate the wave in this case due to a highly noisy environment. The waves are less visible in both the upper part of the tumour in the case of a bi-gel and in the whole tumour when oxygen diffuses only at the top and the bottom figure (6.A.iv). In both cases the proliferation of the tumour is reduced which tends to suggest that a slower proliferation may increase the homoneneity of the environment within the tumour. However, migration speed of the cells in these two cases is very different from one another, suggesting that migration speed is not the main factor controlling this pattern. More investigations are needed to confirm what are the factors influencing this pattern.

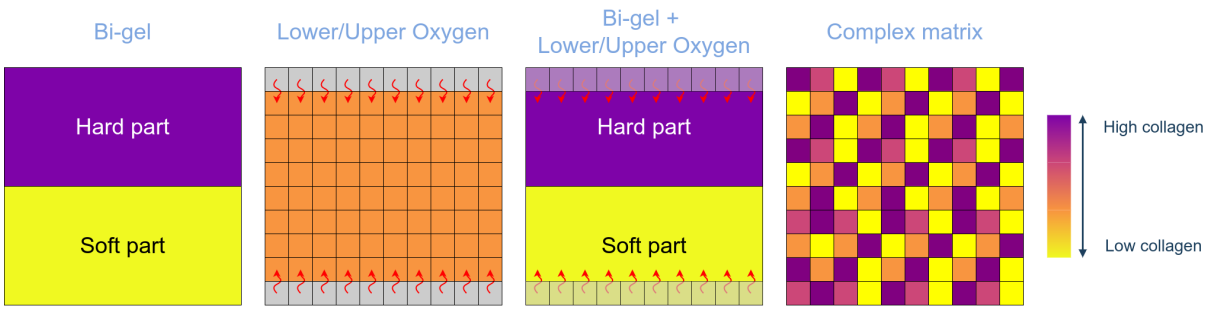

Figure 4: Different environmental settings represented graphically: Bi-Gel with a stiff part and soft part; Lower/Upper oxygen with diffusion at the top and the bottom of the domain; Combination of Bi-Gel and Lower/Upper oxygen; Complex matrix with randomly initiated values of collagen.

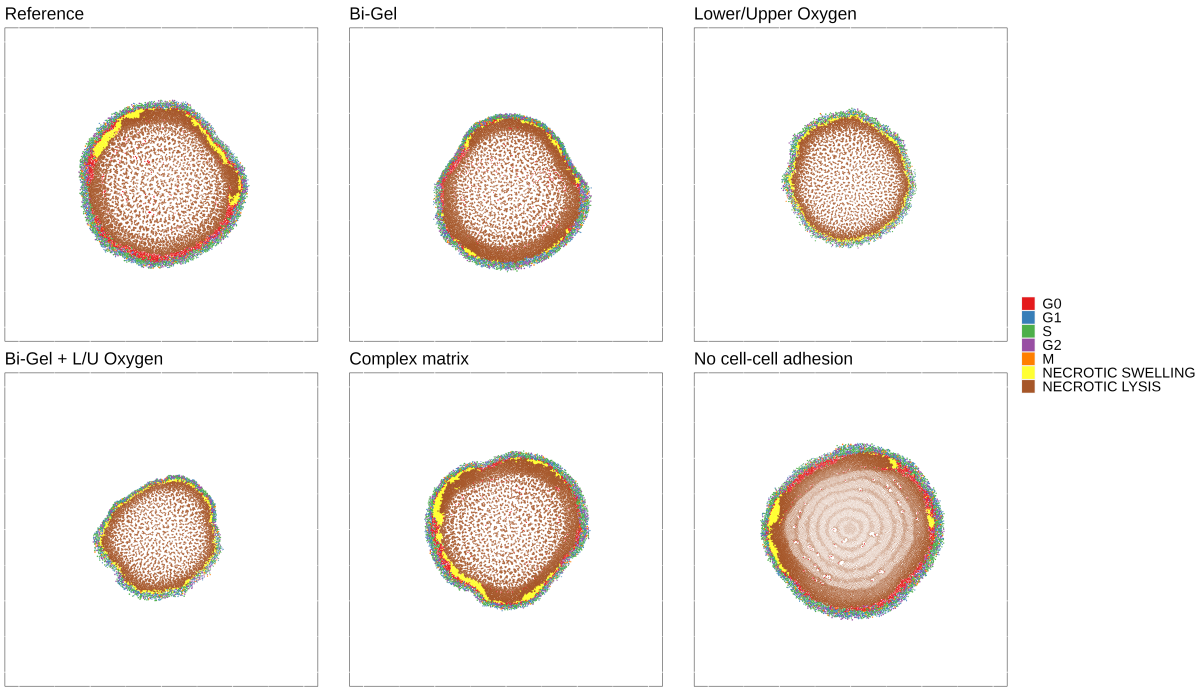

Figure 5: Tumour growth in different conditions with the indication of cell cycle.

As can be seen in figure 7, migration speed in the reference simulation ranges from almost 0 to 0.8 µm/min with most of the values distributed around 0.7 µm/min. Migration was stopped for a few cells in the reference, Bi-Gel and Bi-Gel + Lower/Upper oxygen simulation, as migration speed fall to zero. The simulations where the tumour was grown on a Bi-Gel are the only cases where we can observe two values around which migration speeds seem to aggregate. This is because cells are grown in two different collagen densities depending on whether they are at the top or the bottom of the tumour, enforcing different speeds on the cell. The distribution of migration speed in the complex matrix seems more diverse owing to the random initialization of the matrix. On a homogeneous matrix when oxygen diffuses only at the top and bottom of the domain, migration speed values are comprised between 0.6 and 0.8 which suggests that poorer oxygen conditions strongly select for these values. Probably cells cannot have lower migration speed because they die beforehand due to a lack of nutrients as almost all oxygen is depleted at the end of the simulation.

The impact of the different conditions on proliferation has been determined by the number of cells (living and dead) at the end of the simulation, and the radius of the tumour (see figure 8). The radius of the tumour was calculated by measuring the distance between the centre and the cell the furthest from the center for both the proliferative and the necrotic layers. Tumour growth is maximized in the model when cells have no adhesion and minimized when combining a bi-gel with lower oxygen diffusion. The simulation with no cellular adhesion has the highest number of cells and tumour radius. Taken together, these results show that collagen conditions alone can impact the proliferation of the tumour. Tumour radius and cell number are reduced when oxygen conditions are poorer, showing that oxygen alone can reduce cell proliferation as well. The effect is even more marked when poorer oxygen condition is combined with bi-gel conditions, suggesting a dual effect of both collagen and oxygen.

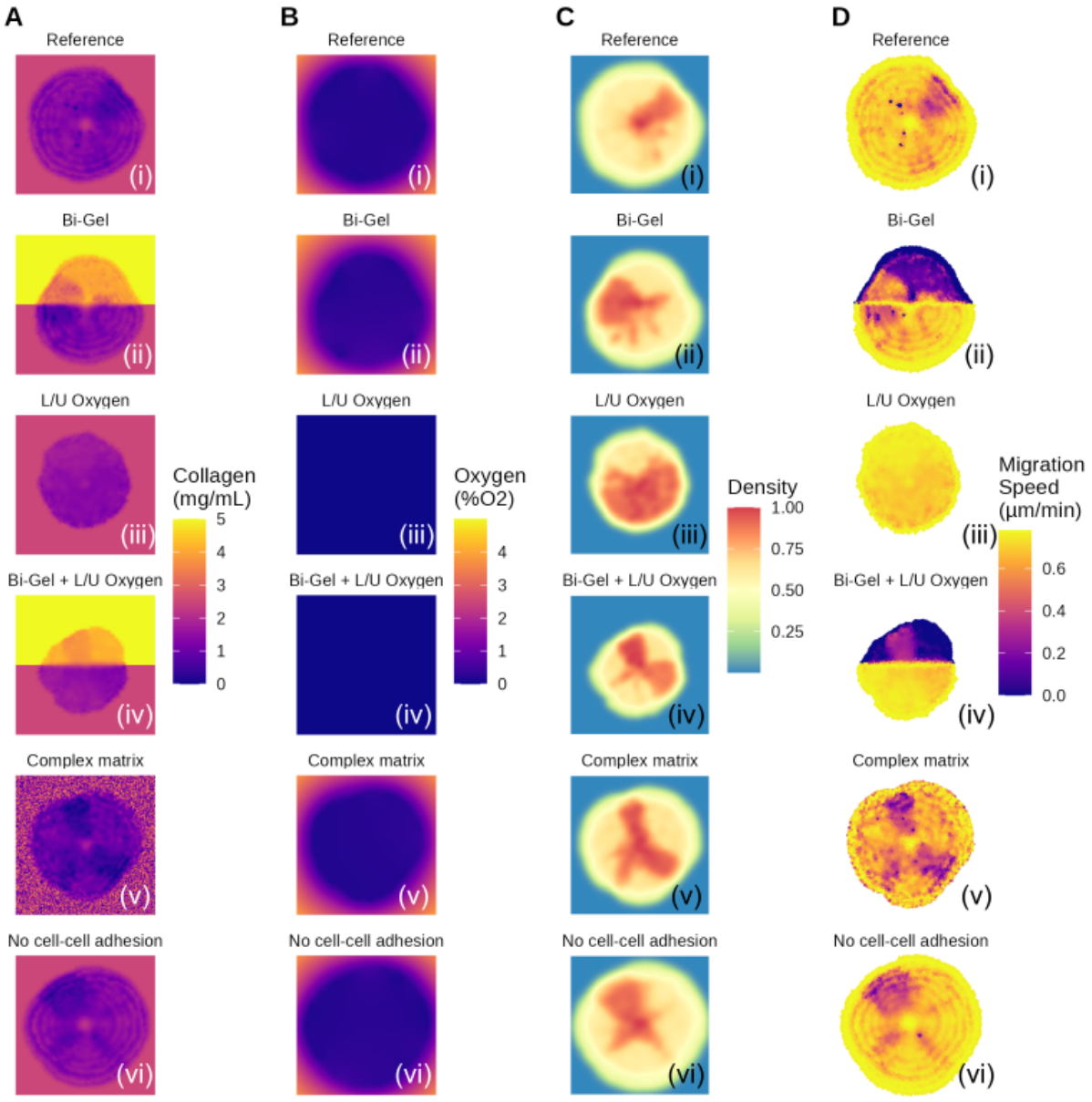

Figure 6: Comparison of (A) the extracellular collagen, (B) extracellular oxygen, (C) the cellular density and (D) the cell migration speed in the different settings studied.

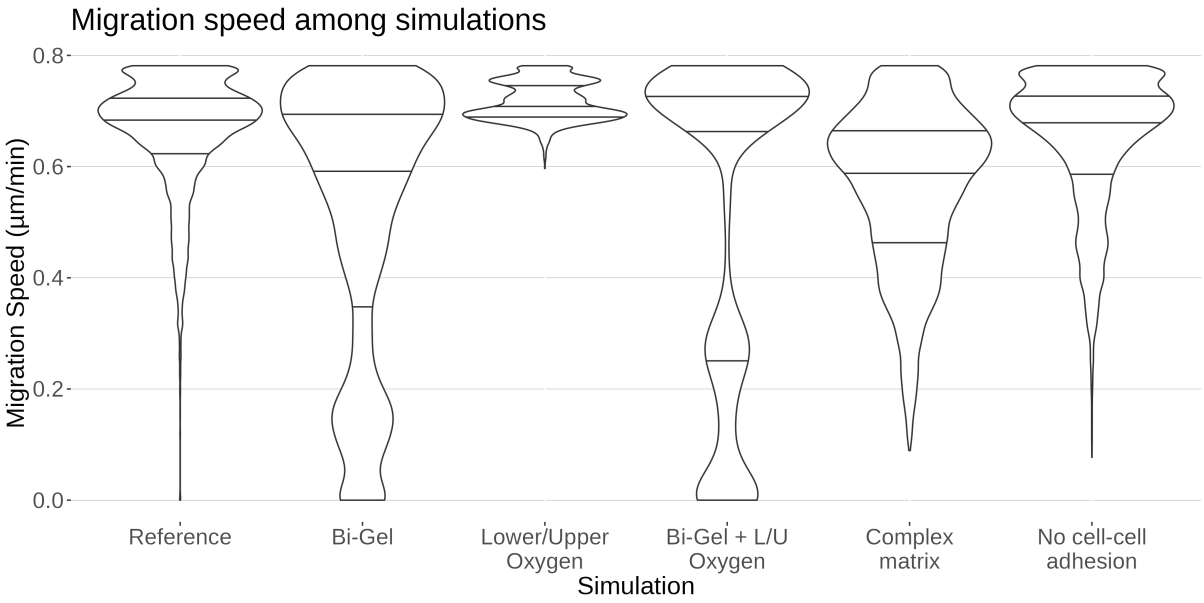

Figure 7: Violin plot of the migration speed in the different collagen conditions.

Extracelullar collagen does not affect the appearance of the Warburg compared to the genetic properties of the cell

The key player of the model in this study is the HIF protein which not only impacts collagen synthesis but the metabolism as well. In previous work [27], we investigated how the interactions between HIF and the metabolic genes LDH and PDH could induce a Warburg Effect. To recall, the Warburg Effect is an increased production of lactate in normoxia. Here we investigated whether extracellular collagen could impact cell metabolism and if conditions that previously triggered the Warburg Effect could lead to the same results. In previous work [27], the Warburg effect could be triggered by reduced HIF degradation by oxygen or through oscillations of oxygen during the simulation. Here we investigated whether this result could be reproduced within the new model. Reduced HIF degradation was simulated by setting $\gamma_{O \to h} = 17.5$. Oscillating conditions correspond to variations of oxygen boundary conditions: simulation starts at normoxic levels (5 % O_2) and then oxygen levels are slowly decreased over six hours to hypoxic levels (1 % O_2). Oxygen levels are then increased back to normoxia at the same rate and the process is repeated until the end of the simulation.

Figure 9 represents the production of H^+ (caused by lactate secretion) depending on the extracellular oxygen level in various simulations. As can be seen, extracellular collagen does not seem to impact the Warburg Effect in the model. Results are similar across the simulation in normoxia. Extracellular oxygen levels fall below 2 % O_2 after only two days and stay below this level in most of the simulation. The lowest values of oxygen levels are reached when the tumour is grown in poorer oxygen conditions. No cells adopted a Warburg phenotype in the Reference, Lower/Upper Oxygen, Complex matrix or Bi-Gel simulations. These results tend to show that collagen has no impact on the Warburg phenotype.

As said above, we ran two simulations in the same conditions that triggered the Warburg Effect in previous work but this did not lead to the adoption of the Warburg phenotype by the cell (results not

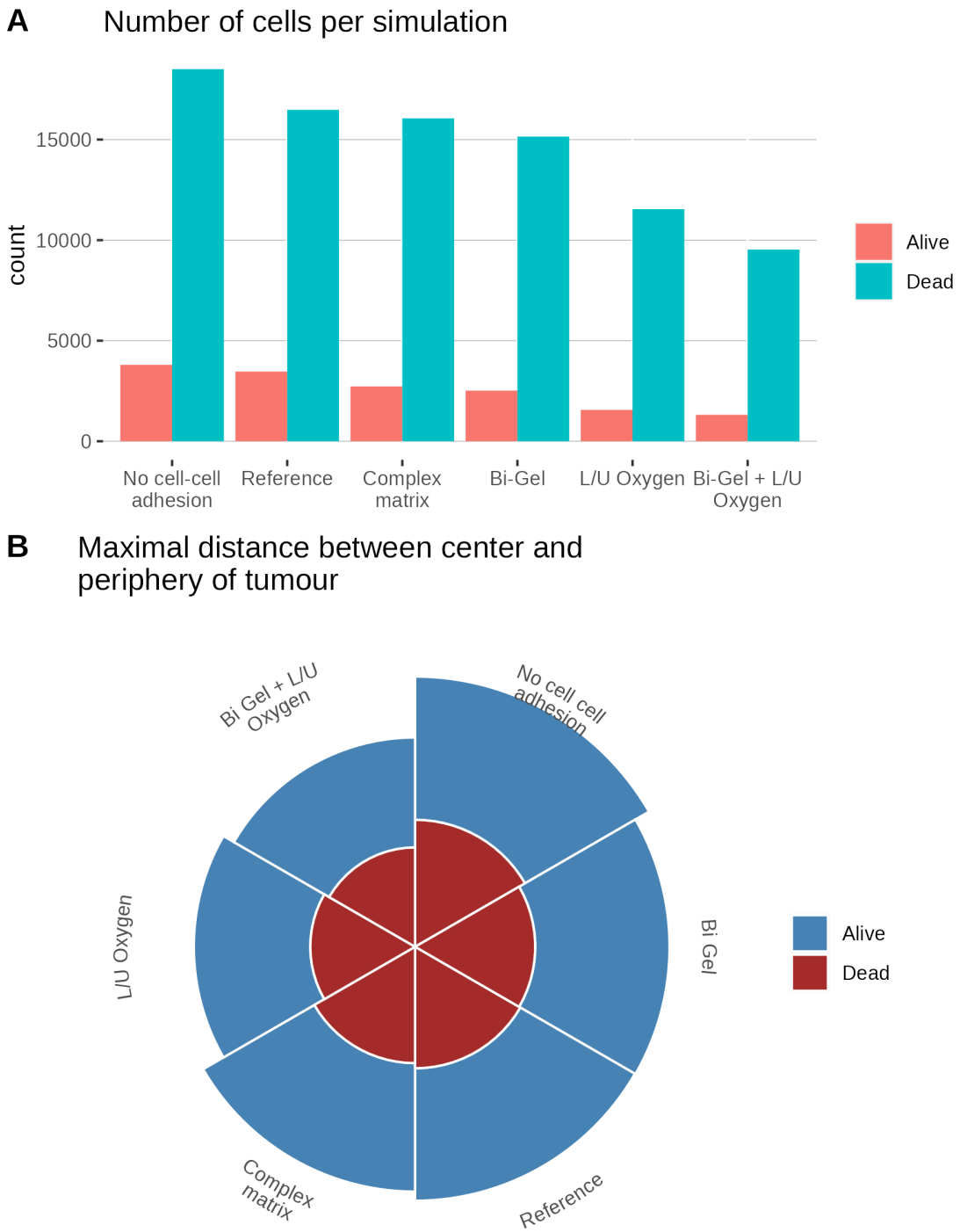

Figure 8: Proliferation of the tumour in the different collagen conditions with (A) a barplot of the number of cells and (B) a pie chart of the maximal proliferation distance. Each slices of the pie chart correspond to a different condition tested, and the height of the slices represent the distance of proliferation which is measured with the radius of the tumour. Hence taller slices represent higher tumour radius. In both cases, the colours represent living and dead cells.

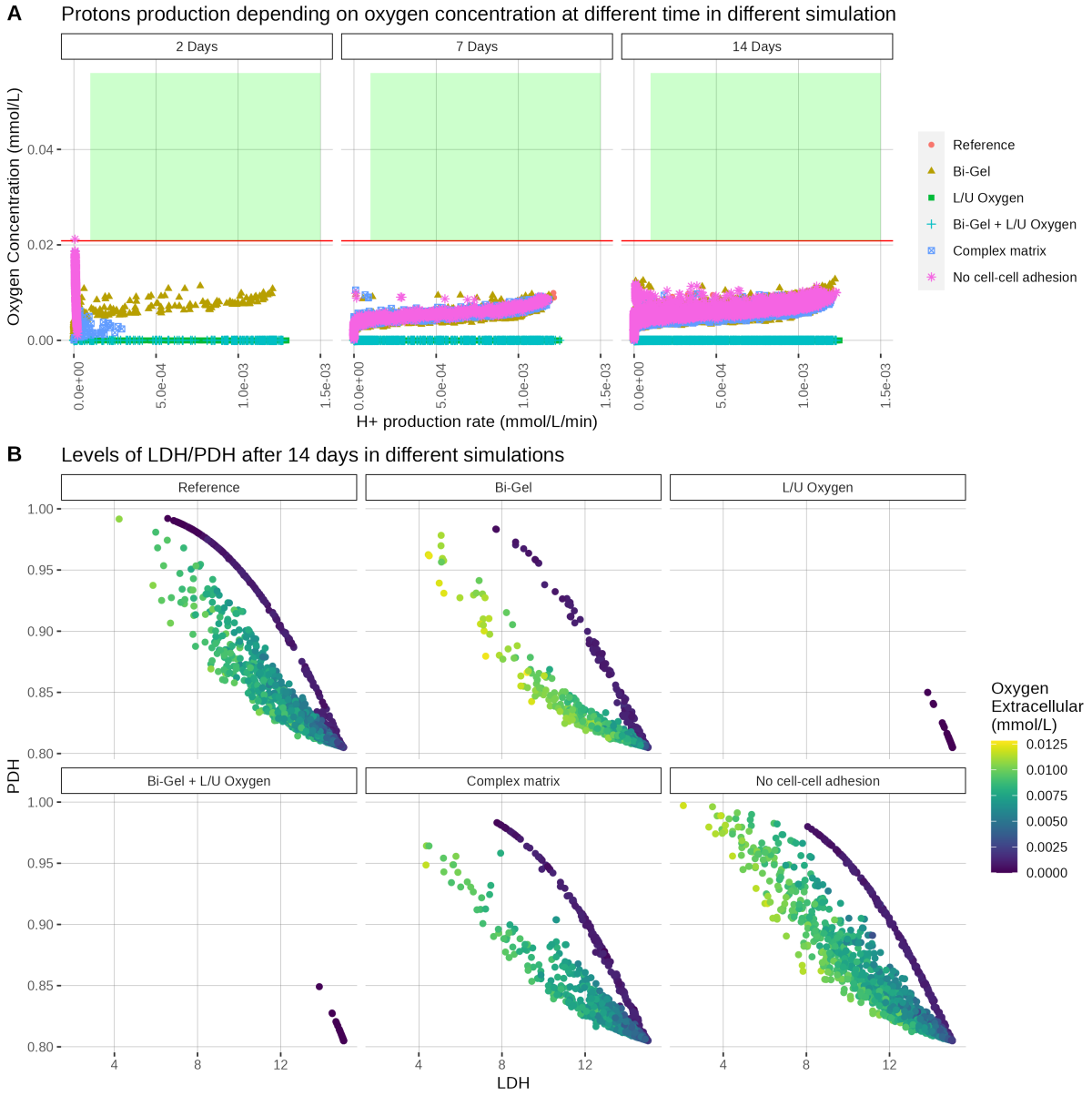

Figure 9: (A) Rate of production of H^+ at 2, 7 and 14 Days and (B) LDH and PDH levels after 14 days of growth, with different collagen or oxygen settings. In (A), only living cells are represented on the graph, the red line indicates the hypoxia threshold (0.02085 mmol/L or 2% O_2) and the green rectangle represents the region corresponding to a Warburg effect.

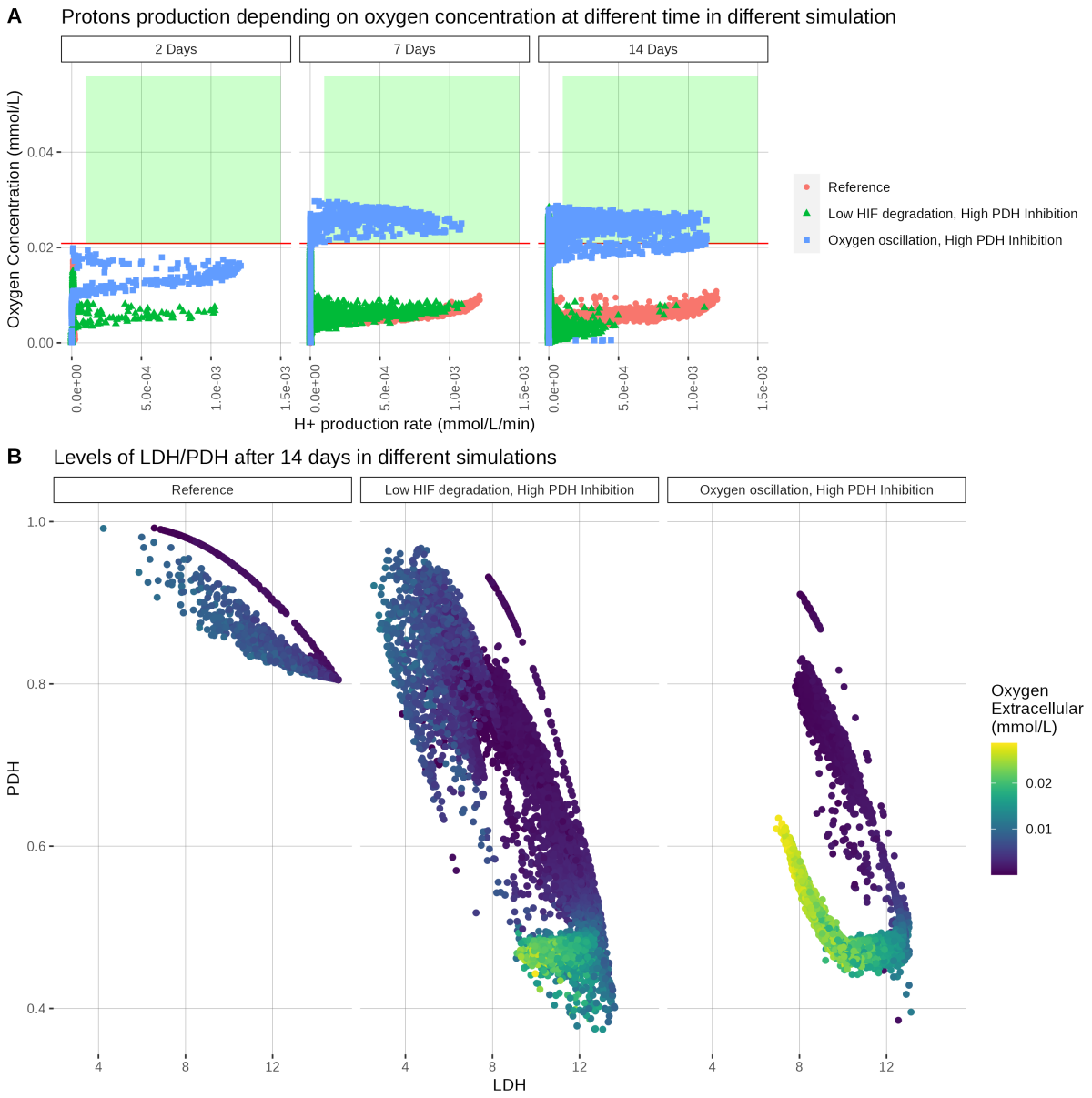

Figure 10: (A) Rate of production of H^+ at 2, 7 and 14 Days and (B) LDH and PDH levels after 14 days of growth, with different genetic settings. In (A), only living cells are represented on the graph, the red line indicates the hypoxia threshold (0.02085 mmol/L or 2% O_2) and the green rectangle represents the region corresponding to a Warburg effect. Low HIF degradation by oxygen is represented by setting $\gamma_{O\to h} = 17.5$. High PDH inhibition is simulated by setting $\gamma_{k\to q} = 0.14$. In oscillating conditions, oxygen concentration is slowly decreased from normoxia (5 % O_2) to severe hypoxia (1 % O_2) during 6h, then oxygen is increased to normoxia at the same rate. This process is repeated until the end of the simulation.

shown). Yet, we noticed that the results of this study are similar to the results obtained in previous work when down-regulation of PDH by pyruvate dehydrogenase kinase (PDK) was decreased. Thus we ran another two simulations with reduced HIF degradation or oxygen oscillation with $\gamma_{k\to q} = 0.14$ to simulate higher inhibition of PDH by PDK. Figure 10 shows the results when inhibition of PDH is higher. Reducing the downregulation of PDH by HIF (through PDK) rescued the adoption of the Warburg phenotype in conditions with oxygen oscillation but not with reduced HIF degradation. This seems to suggest that environmental conditions can trigger the appearance of the Warburg Effect, yet appropriate genetic parameters are necessary. This would explain why the Warburg phenotype was not observed in the result.

Levels of LDH and PDH, shown in figures 9 and 10, seem to support this theory. Three different states can be observed: they correspond to the oxidative state (high PDH/low LDH), the glycolytic state (low PDH/high LDH), and an intermediate state in between the two. This intermediate state is adopted by the cell during its transition from the oxidative to the glycolytic state. LDH/PDH levels follow the same dynamics across the simulations in different collagen conditions. Only the glycolytic cellular state can be observed when oxygen diffuses only at the top and the bottom of the domain, indicating that hypoxia is a strong selector. Lower levels of PDH are attained when increasing the down-regulation of PDH by HIF. This shows that genetic parameters are the main factor affecting the different cellular states in the model. Here, only when oxygen is oscillating and $\gamma_{k\to q} = 0.14$ we can observe cells in the glycolytic state with normoxic oxygen levels.

Discussion

In this paper, we studied the impact of the HIF protein on the extracellular matrix through its effect on the genes involved in the modification of collagen. We extended a model of the impact of HIF on the cellular metabolism previously described [27], with matrix remodeling genes. Literature has demonstrated that HIF is able to up-regulate the genes P4HA1, MT1-MMP and LOX. In the model, P4HA1 modulates the secretion of collagen since this protein catalyzes the post-translational modification important for the self-assembly of collagen fibrils into fibers. In contrast, degradation of collagen in the environment is controlled by MT1-MMP which is an enzyme catalyzing the degradation of collagen fibers through cleavage at specific sites. Finally, we describe two states of collagen namely regular collagen and cross-linked collagen. The cross-linking of collagen is controlled by the LOX enzyme which is the main actor catalyzing the reaction resulting in the formation of cross-links between collagen fibers.

Results have shown a relation between the local cellular density and the extracellular collagen in the environment. This further affects the cellular migration speed which is reduced as there is not enough collagen to ensure optimal migration. This is likely to be due to the higher local cellular density causing an increased degradation of the matrix.

As expected, tumour radius in collagen gels with higher collagen concentration was lower as cell migration was slowed down. Simulation in different collagen conditions demonstrated that it affected the shape of the tumour. Unsurprisingly, when tumour was grown in a Bi-Gel where the extracellular

collagen at the top was higher than at the bottom of the domain, tumour adopted a "pear" shape. As the upper part of the domain has a higher collagen density, cell migration speed and tumour proliferation were reduced. Yet, when tumour growth is initialized on a complex matrix where extracellular collagen varies on each point of the domain, the tumour forms "branching" at the end of the simulation. Tumour proliferation was reduced when collagen density was not optimal for growth and when oxygen conditions were poorer. Interestingly, when diffusion of oxygen at the top and the bottom of the domain was combined with a Bi-Gel, the number of cells at the end of the simulation was further reduced compared to each condition separately. This tends to show a combined effect of oxygen and collagen on cellular proliferation. Different genetic settings for P4HA1, MT1-MMP and LOX were tested to assess their impact on the tumour growth. Yet results did not change significantly, thus we do not show them in the paper.

The Warburg phenotype has been adopted by any cells in the different collagen conditions simulated. This tends to show that collagen is not relevant to the Warburg Effect in the model. Reduced HIF degradation by oxygen and oscillations of oxygen diffusion did not affect the Warburg Effect either. Adoption of the Warburg phenotype by the cells has been rescued only with oscillations of oxygen when the sensitivity of PDH to HIF was higher. This may suggest that inhibition of oxidative metabolism by HIF is the main factor controlling the appearance of the Warburg Effect in the model. Oscillations of oxygen were necessary to induce the Warburg Effect which means that perturbations of oxygenation may still be required. In this regard, the Warburg Effect is thus a combination of environmental and genetic factors.

In this study, tumour growth was simulated only in 2D to limit the computational cost generated by 3D. However, cell migration differs between 2D and 3D as the cell must overcome different pressures in 3D [56]. While extracellular pH is described in the model, its effect on extracellular matrix is not included here. It has been shown that pH can play a role in promoting cellular invasion [57]. For example, MMPs undergo acid-induced activation before they degrade the ECM [58]. Other limitations concern the regulation of MT1-MMP. Firstly, collagen is a molecule able to auto-regulated its own level through a dynamic feedback mechanism that includes regulation of its expression and of the expression of collagen degrading proteinase. At high concentrations, collagen can interact with cell receptors to induce the production of MT1-MMP [41]. Secondly, MT1-MMP self-regulates its activity by cleaving itself, a phenomenon called ectodomain shedding, to remove its catalytic domain which renders MT1-MMP inactive [51, 49]. Here, the regulation of MT1-MMP only includes the effect of HIF and the auto-regulating mechanisms of collagen and MT2-MMP are not described in the model. However, the effect of collagen up-regulation and MT1-MMP auto-regulation could potentially change the results, especially in high or low collagen concentrations. For example, at low collagen concentrations degradation of collagen could be inhibited in order to favour collagen secretion by the cell.

Conclusion

In this paper, we investigated the impact of the HIF protein on the remodeling of the extracellular matrix

through its effect on the three genes P4HA1, MT1-MMP and LOX. We used a mathematical model that combines genetic regulations, metabolism and collagen processes. The model was implemented in an ABM to accurately describe the local impact by the cell. Results have shown that cells tend to degrade the matrix in the model and that a higher local cellular density leads to a lower extra-cellular collagen density. Areas where the cell motility is hindered show, as would be expected, a shorter distance from the center of the tumour. This impacts proliferation as well since a lower total number of cells is observed at the end of the simulation when collagen density is not optimal. Tumour proliferation was reduced when oxygen diffused only at the top or the bottom of the tumour, and it was maximized when cell-cell adhesion was null. Investigation of the effect of different conditions on the Warburg Effect revealed that adoption of the Warburg phenotype by cells was only observed when the sensitivity of PDH to HIF was increased in combination with oscillations of oxygen diffusion at the border of the domain. This seems to suggest that both appropriate environmental conditions and genetic properties of the cell are required for the appearance of the Warburg Effect.

Data availability

Data used for parameter estimation are accessible online on the The Cancer Genome Atlas (TCGA) database in the "TCGA-GBM" project. Data used to estimate the impact of collagen of cellular migration speed were taken from a study from Schol et *al*, 1982 [54].

Acknowledgements

This work is supported by the French National Research Agency in the framework of the "Investissements d'avenir" program (ANR-15-IDEX-02). Kévin Spinicci gratefully acknowledges the support of Swansea University Strategic Partnership Research Scholarship and the support of IDEX Université Grenoble Alpes.

Conflicts of Interest

The authors declare no conflict of interest.

References

[1] Inês G. Gonçalves and Jose Manuel Garcia-Aznar. "Extracellular matrix density regulates the formation of tumour spheroids through cell migration". In: *PLOS Computational Biology* 17.2 (Feb. 26, 2021), e1008764. ISSN: 1553-7358. DOI: 10.1371/journal.pcbi.1008764.

[2] Tamara T. Lah, Metka Novak, and Barbara Breznik. "Brain malignancies: Glioblastoma and brain metastases". In: *Seminars in Cancer Biology* 60 (October 2019 2020), pp. 262–273. ISSN: 10963650. DOI: 10.1016/j.semcancer.2019.10.010.

[3] Achilleas D. Theocharis et al. “Extracellular matrix structure”. In: *Advanced Drug Delivery Reviews*. Extracellular Matrix (ECM) and ECM-like materials: Therapeutic Tools and Targets in Cancer Treatment 97 (Feb. 1, 2016), pp. 4–27. ISSN: 0169-409X. DOI: 10.1016/j.addr.2015.11.001. URL: https://www.sciencedirect.com/science/article/pii/S0169409X15002574 (visited on 08/14/2023).

[4] Hsiang Hsi Hong et al. “A role for lysyl oxidase regulation in the control of normal collagen deposition in differentiating osteoblast cultures”. In: *Journal of Cellular Physiology* 200.1 (July 1, 2004). Publisher: John Wiley & Sons, Ltd, pp. 53–62. ISSN: 1097-4652. DOI: 10.1002/JCP.10476. URL: https://onlinelibrary.wiley.com/doi/full/10.1002/jcp.10476 (visited on 03/27/2023).

[5] Daniele M. Gilkes, Gregg L. Semenza, and Denis Wirtz. “Hypoxia and the extracellular matrix: drivers of tumour metastasis”. In: *Nature Reviews Cancer 2014 14:6* 14.6 (May 15, 2014). Publisher: Nature Publishing Group, pp. 430–439. ISSN: 1474-1768. DOI: 10.1038/nrc3726. URL: https://www.nature.com/articles/nrc3726 (visited on 01/05/2023).

[6] Carmen Chak Lui Wong et al. “Hypoxia-inducible factor 1 is a master regulator of breast cancer metastatic niche formation”. In: *Proceedings of the National Academy of Sciences of the United States of America* 108.39 (Sept. 27, 2011). Publisher: National Academy of Sciences, pp. 16369–16374. ISSN: 00278424. DOI: 10.1073/PNAS.1113483108/SUPPL_FILE/PNAS.201113483SI.PDF. URL: https://www.pnas.org/doi/abs/10.1073/pnas.1113483108 (visited on 01/09/2023).

[7] Stéphane Germain et al. “Hypoxia-driven angiogenesis: Role of tip cells and extracellular matrix scaffolding”. In: *Current Opinion in Hematology* 17.3 (May 2010), pp. 245–251. ISSN: 10656251. DOI: 10.1097/MOH.0B013E32833865B9. URL: https://journals.lww.com/co-hematology/Fulltext/2010/05000/Hypoxia_driven_angiogenesis__role_of_tip_cells_and.15.aspx (visited on 01/06/2023).

[8] Johanna Myllyharju and Ernestina Schipani. “Extracellular matrix genes as hypoxia-inducible targets”. In: *Cell and Tissue Research* 339.1 (Jan. 7, 2010). Publisher: Springer, pp. 19–29. ISSN: 0302766X. DOI: 10.1007/S00441-009-0841-7/FIGURES/3. URL: https://link.springer.com/article/10.1007/s00441-009-0841-7 (visited on 01/06/2023).

[9] Daniela K. Schlüter, Ignacio Ramis-Conde, and Mark A.J. Chaplain. “Computational modeling of single-cell migration: The leading role of extracellular matrix fibers”. In: *Biophysical Journal* 103.6 (Sept. 19, 2012). Publisher: Elsevier, pp. 1141–1151. ISSN: 00063495. DOI: 10.1016/j.bpj.2012.07.048. URL: http://www.cell.com/article/S0006349512008697/fulltext (visited on 01/20/2023).

[10] S. R. McKeown. “Defining normoxia, physoxia and hypoxia in tumours - Implications for treatment response”. In: *British Journal of Radiology* 87.1035 (Mar. 1, 2014). Publisher: British Institute of Radiology. ISSN: 00071285. DOI: 10.1259/bjr.20130676. URL: /pmc/articles/PMC4064601/ (visited on 02/10/2021).

[11] Ana Rita Monteiro et al. “The Role of Hypoxia in Glioblastoma Invasion”. In: *Cells 2017, Vol. 6, Page 45* 6.4 (Nov. 22, 2017). Publisher: Multidisciplinary Digital Publishing Institute, p. 45. ISSN: 2073-4409. DOI: 10.3390/CELLS6040045. URL: https://www.mdpi.com/2073-4409/6/4/45/htm (visited on 01/11/2023).

[12] Eric Leung et al. “Metabolic targeting of HIF-dependent glycolysis reduces lactate, increases oxygen consumption and enhances response to high-dose single-fraction radiotherapy in hypoxic solid tumors”. In: *BMC Cancer* 17.1 (Dec. 15, 2017). Publisher: BioMed Central Ltd., p. 418. ISSN: 1471-2407. DOI: 10.1186/s12885-017-3402-6. URL: https://bmccancer.biomedcentral.com/articles/10.1186/s12885-017-3402-6 (visited on 01/05/2021).

[13] Lucija Slemc and Tanja Kunej. “Transcription factor HIF1A: downstream targets, associated pathways, polymorphic hypoxia response element (HRE) sites, and initiative for standardization of reporting in scientific literature”. In: *Tumor Biology* 37.11 (2016). ISSN: 14230380. DOI: 10.1007/s13277-016-5331-4. URL: https://link.springer.com/article/10.1007/s13277-016-5331-4 (visited on 12/11/2020).

[14] Ji-Won Lee et al. “Hypoxia-inducible factor (HIF -1)alpha : its protein stability and biological function s”. In: *Experimental and Molecular Medicine* 36.1 (2004), pp. 1–12. DOI: 10.1038/emm.2004.1. URL: https://www.nature.com/articles/emm20041.

[15] Georgina N. Masoud and Wei Li. “HIF-1α pathway: Role, regulation and intervention for cancer therapy”. In: *Acta Pharmaceutica Sinica B* 5.5 (2015). ISSN: 22113843. DOI: 10.1016/j.apsb.2015.05.007. URL: https://www.sciencedirect.com/science/article/pii/S2211383515000817?pes=vor (visited on 10/14/2020).

[16] Baptiste Bedessem. “Contributions à l’étude de la réponse moléculaire à l’hypoxie : Modélisation mathématique et expérimentations sur cellules FUCCI”. In: (Oct. 23, 2015). Publisher: Université Grenoble Alpes. URL: https://theses.hal.science/tel-01318127 (visited on 08/09/2023).

[17] Laura D’Ignazio, Michael Batie, and Sonia Rocha. “Hypoxia and inflammation in cancer, focus on HIF and NF-ϰB”. In: *Biomedicines* 5.2 (June 1, 2017). Publisher: MDPI AG. ISSN: 22279059. DOI: 10.3390/biomedicines5020021. URL: /pmc/articles/PMC5489807/?report=abstract (visited on 10/21/2020).

[18] Hui Xu et al. “Activation of hypoxia signaling induces phenotypic transformation of glioma cells: implications for bevacizumab antiangiogenic therapy”. In: *Oncotarget* 6.14 (Mar. 14, 2015). Publisher: Impact Journals, pp. 11882–11893. ISSN: 1949-2553. DOI: 10.18632/ONCOTARGET.3592. URL: https://www.oncotarget.com/article/3592/text/ (visited on 01/12/2023).

[19] Daniela K. Schlüter, Ignacio Ramis-Conde, and Mark A.J. Chaplain. “Multi-scale modelling of the dynamics of cell colonies: insights into cell-adhesion forces and cancer invasion from in silico simulations”. In: *Journal of The Royal Society Interface* 12.103 (Feb. 6, 2015). Publisher: The Royal Society. ISSN: 17425662. DOI: 10.1098/RSIF.2014.1080. URL: https://royalsocietypublishing.org/doi/10.1098/rsif.2014.1080 (visited on 01/20/2023).

[20] Alexander R.A. Anderson. "A hybrid mathematical model of solid tumour invasion: the importance of cell adhesion". In: *Mathematical medicine and biology : a journal of the IMA* 22.2 (2005). Publisher: Math Med Biol, pp. 163–186. ISSN: 1477-8599. DOI: 10.1093/IMAMMB/DQI005. URL: https://pubmed.ncbi.nlm.nih.gov/15781426/ (visited on 01/10/2022).

[21] Niall E. Deakin and Mark A.J. Chaplain. "Mathematical modeling of cancer invasion: The role of membrane-bound matrix metalloproteinases". In: *Frontiers in Oncology* 3 APR (Apr. 3, 2013). Publisher: Frontiers, p. 70. ISSN: 2234943X. DOI: 10.3389/FONC.2013.00070/ABSTRACT. (Visited on 01/20/2023).

[22] Brenda M. Rubenstein and Laura J. Kaufman. "The Role of Extracellular Matrix in Glioma Invasion: A Cellular Potts Model Approach". In: *Biophysical Journal* 95.12 (Dec. 15, 2008). Publisher: Cell Press, pp. 5661–5680. ISSN: 0006-3495. DOI: 10.1529/BIOPHYSJ.108.140624. (Visited on 03/27/2023).

[23] Miguel AS Cavadas, Lan K. Nguyen, and Alex Cheong. "Hypoxia-inducible factor (HIF) network: insights from mathematical models". In: *Cell Communication and Signaling* 11.1 (June 10, 2013), p. 42. ISSN: 1478-811X. DOI: 10.1186/1478-811X-11-42. URL: https://doi.org/10.1186/1478-811X-11-42 (visited on 09/28/2023).

[24] B. Bedessem and A. Stéphanou. "A mathematical model of HiF-1α-mediated response to hypoxia on the G1/S transition". In: *Mathematical Biosciences* 248.1 (2014). Publisher: Elsevier Inc., pp. 31–39. ISSN: 00255564. DOI: 10.1016/j.mbs.2013.11.007. URL: http://dx.doi.org/10.1016/j.mbs.2013.11.007.

[25] Baptiste Bedessem and Angélique Stéphanou. "Role of compartmentalization on HiF-1α degradation dynamics during changing oxygen conditions: A computational approach". In: *PLoS ONE* 9.10 (Oct. 22, 2014). Publisher: Public Library of Science, p. 110495. ISSN: 19326203. DOI: 10.1371/journal.pone.0110495. URL: https://journals.plos.org/plosone/article?id=10.1371/journal.pone.0110495 (visited on 01/13/2021).

[26] Dongya Jia et al. "Elucidating cancer metabolic plasticity by coupling gene regulation with metabolic pathways". In: *Proceedings of the National Academy of Sciences of the United States of America* 116.9 (Feb. 26, 2019). Publisher: National Academy of Sciences, pp. 3909–3918. ISSN: 10916490. DOI: 10.1073/pnas.1816391116. URL: https://pubmed.ncbi.nlm.nih.gov/30733294/ (visited on 12/18/2020).

[27] Kévin Spinicci et al. "Modeling the role of HIF in the regulation of metabolic key genes LDH and PDH: Emergence of Warburg phenotype". In: *Computational and Systems Oncology* 2.3 (Sept. 1, 2022). Publisher: John Wiley & Sons, Ltd, e1040. ISSN: 2689-9655. DOI: 10.1002/CSO2.1040. URL: https://onlinelibrary.wiley.com/doi/full/10.1002/cso2.1040 (visited on 08/25/2022).

[28] Arabel Vollmann-Zwerenz et al. "Tumor Cell Invasion in Glioblastoma". In: *International Journal of Molecular Sciences 2020, Vol. 21, Page 1932* 21.6 (Mar. 12, 2020). Publisher: Multidisciplinary Digital Publishing Institute, p. 1932. ISSN: 1422-0067. DOI: 10.3390/IJMS21061932. URL: https://www.mdpi.com/1422-0067/21/6/1932/htm (visited on 01/09/2023).

[29] Laura J. Kaufman et al. “Glioma expansion in collagen I matrices: Analyzing collagen concentration-dependent growth and motility patterns”. In: *Biophysical Journal* 89.1 (2005). Publisher: Elsevier, pp. 635–650. ISSN: 00063495. DOI: 10.1529/biophysj.105.061994. URL: http://dx.doi.org/10.1529/biophysj.105.061994.

[30] Pranita Kaphle, Yongchao Li, and Li Yao. “The mechanical and pharmacological regulation of glioblastoma cell migration in 3D matrices”. In: *Journal of Cellular Physiology* 234.4 (2019), pp. 3948–3960. ISSN: 10974652. DOI: 10.1002/jcp.27209.

[31] Wenbo Li and Jin Wang. “Uncovering the Underlying Mechanisms of Cancer Metabolism through the Landscapes and Probability Flux Quantifications”. In: *iScience* 23.4 (Apr. 24, 2020). Publisher: Elsevier Inc., p. 101002. ISSN: 25890042. DOI: 10.1016/j.isci.2020.101002. URL: https://doi.org/10.1016/j.isci.2020.101002 (visited on 02/12/2021).

[32] Mark Robertson-Tessi et al. “Impact of Metabolic Heterogeneity on Tumor Growth, Invasion, and Treatment Outcomes”. In: *Cancer Research* 75.8 (Apr. 15, 2015). Publisher: American Association for Cancer Research Inc., pp. 1567–1579. ISSN: 0008-5472. DOI: 10.1158/0008-5472.CAN-14-1428. URL: http://cancerres.aacrjournals.org/lookup/doi/10.1158/0008-5472.CAN-14-1428 (visited on 05/19/2021).

[33] Ahmadreza Ghaffarizadeh et al. “PhysiCell: An open source physics-based cell simulator for 3-D multicellular systems”. In: *PLOS Computational Biology* 14.2 (Feb. 1, 2018). Publisher: Public Library of Science, e1005991. ISSN: 1553-7358. DOI: 10.1371/JOURNAL.PCBI.1005991. URL: https://journals.plos.org/ploscompbiol/article?id=10.1371/journal.pcbi.1005991 (visited on 09/16/2021).

[34] Gaofeng Xiong et al. “Collagen prolyl 4-hydroxylase 1 is essential for HIF-1α stabilization and TNBC chemoresistance”. In: *Nature Communications 2018 9:1* 9.1 (Oct. 26, 2018). Publisher: Nature Publishing Group, pp. 1–16. ISSN: 2041-1723. DOI: 10.1038/s41467-018-06893-9. URL: https://www.nature.com/articles/s41467-018-06893-9 (visited on 01/09/2023).

[35] Ming Zhu Jin and Wei Lin Jin. “The updated landscape of tumor microenvironment and drug repurposing”. In: *Signal Transduction and Targeted Therapy 2020 5:1* 5.1 (Aug. 25, 2020). Publisher: Nature Publishing Group, pp. 1–16. ISSN: 2059-3635. DOI: 10.1038/s41392-020-00280-x. URL: https://www.nature.com/articles/s41392-020-00280-x (visited on 01/18/2023).

[36] Christopher J. Brereton et al. “Pseudohypoxic HIF pathway activation dysregulates collagen structure-function in human lung fibrosis”. In: *eLife* 11 (Feb. 1, 2022). Publisher: eLife Sciences Publications Ltd. ISSN: 2050084X. DOI: 10.7554/ELIFE.69348. (Visited on 01/05/2023).

[37] Jing Lin et al. “P4HA2 Promotes Epithelial-to-Mesenchymal Transition and Glioma Malignancy through the Collagen-Dependent PI3K/AKT Pathway”. In: *Journal of Oncology* 2021 (2021). Publisher: Hindawi Limited. ISSN: 16878469. DOI: 10.1155/2021/1406853. (Visited on 01/10/2023).

[38] Wenjun Guo and Filippo G. Giancotti. "Integrin signalling during tumour progression". In: *Nature Reviews Molecular Cell Biology 2004 5:10* 5.10 (Oct. 2004). Publisher: Nature Publishing Group, pp. 816–826. ISSN: 1471-0080. DOI: 10.1038/nrm1490. URL: https://www.nature.com/articles/nrm1490 (visited on 08/30/2022).

[39] Sabrina Amar, Lyndsay Smith, and Gregg B. Fields. "Matrix metalloproteinase collagenolysis in health and disease". In: *Biochimica et Biophysica Acta (BBA) - Molecular Cell Research* 1864.11 (Nov. 1, 2017). Publisher: Elsevier, pp. 1940–1951. ISSN: 0167-4889. DOI: 10.1016/J.BBAMCR.2017.04.015. (Visited on 06/06/2023).

[40] Giuseppe Musumeci et al. "Characterization of matrix metalloproteinase-2 and -9, ADAM-10 and N-cadherin expression in human glioblastoma multiforme". In: *Cell and Tissue Research* 362.1 (Oct. 22, 2015). Publisher: Springer Verlag, pp. 45–60. ISSN: 14320878. DOI: 10.1007/S00441-015-2197-5/TABLES/2. URL: https://link.springer.com/article/10.1007/s00441-015-2197-5 (visited on 01/17/2023).

[41] Eric M. Tam et al. "Characterization of the Distinct Collagen Binding, Helicase and Cleavage Mechanisms of Matrix Metalloproteinase 2 and 14 (Gelatinase A and MT1-MMP)". In: *Journal of Biological Chemistry* 279.41 (Oct. 8, 2004). Publisher: Elsevier BV, pp. 43336–43344. ISSN: 00219258. DOI: 10.1074/jbc.m407186200. URL: http://www.jbc.org/article/S0021925820770894/fulltext (visited on 06/02/2023).

[42] M. Aktar Ali et al. "SNS-032 prevents hypoxia-mediated glioblastoma cell invasion by inhibiting hypoxia inducible factor-1α expression". In: *International Journal of Oncology* 34.4 (Apr. 1, 2009). Publisher: Spandidos Publications, pp. 1051–1060. ISSN: 10196439. DOI: 10.3892/IJO_00000231/HTML. URL: http://www.spandidos-publications.com/10.3892/ijo_00000231/abstract (visited on 01/06/2023).

[43] Brenda L. Petrella, Jouko Lohi, and Constance E. Brinckerhoff. "Identification of membrane type-1 matrix metalloproteinase as a target of hypoxia-inducible factor-2α in von Hippel–Lindau renal cell carcinoma". In: *Oncogene* 24.6 (Feb. 2005). Number: 6 Publisher: Nature Publishing Group, pp. 1043–1052. ISSN: 1476-5594. DOI: 10.1038/sj.onc.1208305. URL: https://www.nature.com/articles/1208305 (visited on 10/03/2023).

[44] Jun Wan et al. "HIF-1α effects on angiogenic potential in human small cell lung carcinoma". In: *Journal of Experimental & Clinical Cancer Research* 30.1 (Dec. 2011). Number: 1 Publisher: BioMed Central, pp. 1–14. ISSN: 1756-9966. DOI: 10.1186/1756-9966-30-77. URL: https://jeccr.biomedcentral.com/articles/10.1186/1756-9966-30-77 (visited on 10/03/2023).

[45] Takeharu Sakamoto and Motoharu Seiki. "Integrated functions of membrane-type 1 matrix metalloproteinase in regulating cancer malignancy: Beyond a proteinase". In: *Cancer Science* 108.6 (2017). _eprint: https://onlinelibrary.wiley.com/doi/pdf/10.1111/cas.13231, pp. 1095–1100. ISSN: 1349-7006. DOI: 10.1111/cas.13231. URL: https://onlinelibrary.wiley.com/doi/abs/10.1111/cas.13231 (visited on 10/03/2023).

[46] Sandeep Unwith et al. “The potential role of HIF on tumour progression and dissemination”. In: *International Journal of Cancer* 136.11 (2015). _eprint: https://onlinelibrary.wiley.com/doi/pdf/10.1002/ijc.28889, pp. 2491–2503. ISSN: 1097-0215. DOI: 10.1002/ijc.28889. URL: https://onlinelibrary.wiley.com/doi/abs/10.1002/ijc.28889 (visited on 10/03/2023).

[47] Rahimsan K. Ramachandran et al. “Expression and prognostic impact of matrix metalloproteinase-2 (MMP-2) in astrocytomas”. In: *PLOS ONE* 12.2 (Feb. 1, 2017). Publisher: Public Library of Science ISBN: 1111111111, e0172234. ISSN: 1932-6203. DOI: 10.1371/JOURNAL.PONE.0172234. URL: https://journals.plos.org/plosone/article?id=10.1371/journal.pone.0172234 (visited on 01/17/2023).

[48] J. Varani et al. “Collagenolytic and gelatinolytic matrix metalloproteinases and their inhibitors in basal cell carcinoma of skin: comparison with normal skin”. In: *British Journal of Cancer 2000 82:3* 82.3 (Jan. 7, 2000). Publisher: Nature Publishing Group, pp. 657–665. ISSN: 1532-1827. DOI: 10.1054/bjoc.1999.0978. URL: https://www.nature.com/articles/6690978 (visited on 06/05/2023).

[49] Yoshifumi Itoh and Motoharu Seiki. “MT1-MMP: A potent modifier of pericellular microenvironment”. In: *Journal of Cellular Physiology* 206.1 (Jan. 1, 2006). Publisher: John Wiley & Sons, Ltd, pp. 1–8. ISSN: 1097-4652. DOI: 10.1002/JCP.20431. URL: https://onlinelibrary.wiley.com/doi/full/10.1002/jcp.20431 (visited on 06/09/2023).

[50] Daisuke Hoshino et al. “Establishment and Validation of Computational Model for MT1-MMP Dependent ECM Degradation and Intervention Strategies”. In: *PLOS Computational Biology* 8.4 (2012). Publisher: Public Library of Science, e1002479. ISSN: 1553-7358. DOI: 10.1371/JOURNAL.PCBI.1002479. URL: https://journals.plos.org/ploscompbiol/article?id=10.1371/journal.pcbi.1002479 (visited on 04/06/2023).

[51] Emmanouil D. Karagiannis and Aleksander S. Popel. “A theoretical model of type I collagen proteolysis by matrix metalloproteinase (MMP) 2 and membrane type 1 MMP in the presence of tissue inhibitor of metalloproteinase 2”. In: *Journal of Biological Chemistry* 279.37 (Sept. 10, 2004). Publisher: Elsevier, pp. 39105–39114. ISSN: 00219258. DOI: 10.1074/jbc.M403627200. URL: http://www.jbc.org/article/S0021925820729674/fulltext (visited on 05/31/2023).

[52] Michael I. Love, Wolfgang Huber, and Simon Anders. “Moderated estimation of fold change and dispersion for RNA-seq data with DESeq2”. In: *Genome Biology* 15.12 (Dec. 5, 2014). Publisher: BioMed Central Ltd., pp. 1–21. ISSN: 1474760X. DOI: 10.1186/s13059-014-0550-8. URL: https://link.springer.com/article/10.1186/s13059-014-0550-8 (visited on 11/04/2020).

[53] Aalpen A. Patel et al. “A cellular automaton model of early tumor growth and invasion: The effects of native tissue vascularity and increased anaerobic tumor metabolism”. In: *Journal of Theoretical Biology* 213.3 (Dec. 7, 2001). Publisher: Academic Press, pp. 315–331. ISSN: 00225193. DOI: 10.1006/jtbi.2001.2385. (Visited on 06/07/2021).

[54] Seth L. Schor et al. “The use of three-dimensional collagen gels for the study of tumour cell invasion in vitro: Experimental parameters influencing cell migration into the gel matrix”. In: *International Journal of Cancer* 29.1 (Jan. 15, 1982). Publisher: John Wiley & Sons, Ltd, pp. 57–62. ISSN: 1097-0215. DOI: 10.1002/IJC.2910290110. URL: https://onlinelibrary.wiley.com/doi/full/10.1002/ijc.2910290110 (visited on 02/23/2023).

[55] Karin Pfisterer et al. “The Extracellular Matrix in Skin Inflammation and Infection”. In: *Frontiers in Cell and Developmental Biology* 9 (2021). ISSN: 2296-634X. URL: https://www.frontiersin.org/articles/10.3389/fcell.2021.682414 (visited on 08/25/2023).

[56] Nadine R. Lang et al. “Biphasic response of cell invasion to matrix stiffness in three-dimensional biopolymer networks”. In: *Acta Biomaterialia* 13 (Feb. 1, 2015). Publisher: Elsevier, pp. 61–67. ISSN: 1742-7061. DOI: 10.1016/J.ACTBIO.2014.11.003. (Visited on 02/28/2023).

[57] Veronica Estrella et al. “Acidity generated by the tumor microenvironment drives local invasion”. In: *Cancer Research* 73.5 (Mar. 1, 2013). Publisher: American Association for Cancer Research, pp. 1524–1535. ISSN: 00085472. DOI: 10.1158/0008-5472.CAN-12-2796/650773/AM/ACIDITY-GENERATED-BY-THE-TUMOR-MICROENVIRONMENT. URL: https://aacrjournals.org/cancerres/article/73/5/1524/586608/Acidity-Generated-by-the-Tumor-Microenvironment (visited on 01/18/2023).

[58] Ebbe Boedtkjer and Stine F. Pedersen. “The Acidic Tumor Microenvironment as a Driver of Cancer”. In: *https://doi.org/10.1146/annurev-physiol-021119-034627* 82 (Feb. 10, 2020). Publisher: Annual Reviews, pp. 103–126. ISSN: 15451585. DOI: 10.1146/ANNUREV-PHYSIOL-021119-034627. URL: https://www.annualreviews.org/doi/abs/10.1146/annurev-physiol-021119-034627 (visited on 01/12/2023).